THE JOURNAL OF PHYSICAL CHEMISTRY B
A JOURNAL OF THE AMERICAN CHEMICAL SOCIETY

pubs.acs.org/JPCB

Article

Structure–Thermodynamic Relationship of a Polysaccharide Gel (Alginate) as a Function of Water Content and Counterion Type (Na vs Ca)

Avery A. Agles* and Ian C. Bourg

Cite This: *J. Phys. Chem. B* 2023, 127, 1828–1841

Read Online

ACCESS | Metrics & More | Article Recommendations | Supporting Information

ABSTRACT: Biofilms are the predominant mode of microbial life on Earth, and so a deep understanding of microbial communities—and their impacts on environmental processes—requires a firm understanding of biofilm properties. Because of the importance of biofilms to their microbial inhabitants, microbes have evolved different ways of engineering and reconfiguring the matrix of extracellular polymeric substances (EPS) that constitute the main non-living component of biofilms. This ability makes it difficult to distinguish between the biotic and abiotic origins of biofilm properties. An important route toward establishing this distinction has been the study of simplified models of the EPS matrix. This study builds on such efforts by using atomistic simulations to predict the nanoscale (≤10 nm scale) structure of a model EPS matrix and the sensitivity of this structure to interpolymer interactions and water content. To accomplish this, we use replica exchange molecular dynamics (REMD) simulations to generate all-atom configurations of ten 3.4 kDa alginate polymers at a range of water contents and Ca–Na ratios. Simulated systems are solvated with explicitly modeled water molecules, which allows us to capture the discrete structure of the hydrating water and to examine the thermodynamic stability of water in the gels as they are progressively dehydrated. Our primary findings are that (i) the structure of the hydrogels is highly sensitive to the identity of the charge-compensating cations, (ii) the thermodynamics of water within the gels (specific enthalpy and free energy) are, surprisingly, only weakly sensitive to cation identity, and (iii) predictions of the differential enthalpy and free energy of hydration include a short-ranged enthalpic term that promotes hydration and a longer-ranged (presumably entropic) term that promotes dehydration, where short and long ranges refer to distances shorter or longer than ∼0.6 nm between alginate strands.

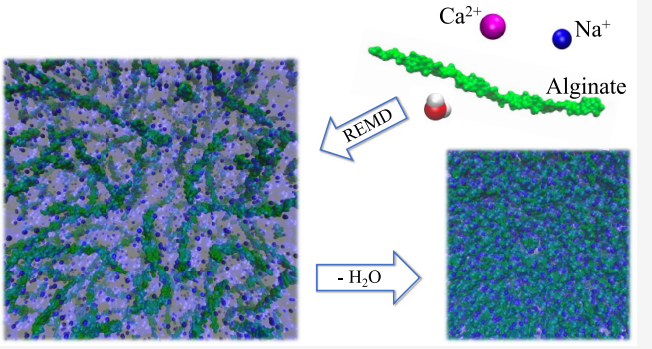

INTRODUCTION

Microbial life in all environments, from oceans to soils to the human body, primarily and most actively exists inside the subenvironment of a biofilm.[1] Termed "stiff water" by early investigators,[2] biofilms are hydrated gel networks of biomolecules that are broadly referred to as extracellular polymeric substances (EPS).[3,4] Of the EPS, polysaccharides are thought to play a key role in a biofilm's structural coherence[5−8] and resistance to water stress,[9−11] yet the fundamental mechanisms whereby polysaccharides confer these properties remain incompletely understood. This knowledge gap represents a critical bottleneck in efforts to understand the larger scale properties of biofilms, such as the spatial and temporal gradients of organisms and extracellular molecules that result in a supraorganism, wherein multiple generations of microorganisms can specialize and cooperate.[12−14]

A key aspect of the structural coherence of biofilms is the persistence of spatiotemporal gradients sharp enough to be described as "microdomains".[15] On the length scale of a few to tens of micrometers,[16] these microdomains further compartmentalize extracellular activity within the biofilm and include water-rich pores that can buffer the cells from fluctuations in water availability.[2,17,18] In instances where the microorganisms and EPS proliferate concurrently, these heterogeneities in the distribution of biofilm cells have been somewhat explained by the well-known depletion aggregation that occurs in colloid–polymer mixtures.[19,20] This "macromolecular crowding" phenomenon results in regions of high cell density separated by regions of high macromolecular density[21] and can give rise to water-filled macropores in the EPS matrix when the cells die or coordinate a dispersal.[18] However, whereas these cellular processes can explain the *formation* of macropores on length

Received: October 10, 2022
Revised: January 31, 2023
Published: February 15, 2023

https://doi.org/10.1021/acs.jpcb.2c07129
J. Phys. Chem. B 2023, 127, 1828–1841

scales greater than a single cell, they cannot on their own explain the *persistence* of these pores or related phenomena such as the response of the biofilm as a whole to variations in the external water potential or aqueous chemistry. Observations that EPS secretions protect cells from water stress even in single-cell systems[22] suggest that a key role is also played by the nanoscale (molecular level) properties of the EPS matrix. In short, a detailed understanding of the biofilm structure and large-scale properties likely requires knowledge of both the microbial level processes on scales of 10^{-6} to 10^{-5} m that generate structure (cell growth, death, and dispersal) and the molecular level properties of polysaccharide gels on scales of 10^{-9} to 10^{-7} m that provide coherence and desiccation resistance.

The extracellular space of biofilms is essentially a solution of polymers—mostly polyelectrolytes—with varying degrees of association and cross-linking,[23] and so we posit that insight into the microstructural heterogeneities in the biofilm matrix can be gained by investigating how polymer−polymer, polymer−water, and water−water interactions result in molecular structures, mechanics, and energetics on scales below 10 nm. This idea is supported by the results of recent investigations into the distinct impacts of divalent versus monovalent inorganic cations on key biofilm properties including mechanical stability, permeability, and bioactivity.[24−29] Divalent cations are of interest because they can provide labile cross-linkages between negatively charged polysaccharide molecules, thus impacting the molecular architecture of the biofilm matrix.[30] These microscale impacts influence larger-scale microbial strategies as illustrated by the bacterial species *Pseudomonas aeruginosa*, which produces biofilms with the polyanionic polysaccharide alginate, for which certain virulence factors—including those which regulate biofilm production—are highly sensitive to aqueous Ca^{2+} concentrations.[31,32] In addition, microorganisms in wastewater treatment facilities have been observed secreting greater amounts of polysaccharides when exposed to higher levels of calcium.[24] Together, these results suggest that the microstructure and macroscopic-level properties of EPS gels are impacted more-or-less directly by molecular-level processes and notably by polymer cross-linking by divalent cations.

Insights into the fundamental properties of polysaccharides and EPS gels have been generated using a variety of methods including rheology,[33−36] permeability,[37−39] swelling pressure measurements,[40,41] electron microscopy visualization of the nanoscale architecture,[42,43] and theories of associating polyelectrolytes.[44,45] A limitation of these techniques, however, is that they do not resolve effects associated with the discrete nature of the solvent. This limitation is potentially significant, in that the inside of polysaccharide gels forms a nanoporous medium with pore size on the order of a few nanometers. Studies of water in nanofluidic devices,[46−49] reverse micelles,[50] biological membrane channels,[51] and other nanoporous systems[52−56] reveal that liquid water adopts properties distinct from those of bulk liquid water when confined in pores smaller than about 2 nm,[57] and that molecular-level information is required to understand these properties.

Molecular dynamics (MD) simulations provide a means of probing atomistic scale phenomena and are currently one of the primary tools employed to resolve the architecture of aqueous biopolymers as topologically heterogeneous as proteins[58,59] and natural organic matter.[60−62] In the case of biopolymer solutions, a key limitation of this approach is that current computational capabilities constrain the time and length scales of simulations to hundreds of nanoseconds and tens of nanometers, orders of magnitude below the time and length scales required to explore the conformational relaxation of polymeric macromolecules or the spatial heterogeneities noted above.

Computational sampling techniques aim to overcome the challenge outlined above by using either coarse-grained representations of the simulated systems[63,64] or, alternatively, approaches that accelerate the exploration of the energetic landscape of the system.[65,66] The replica exchange molecular dynamics (REMD) technique, also known as parallel tempering, has emerged as one of the primary methods used by computational biologists to ascertain the equilibrium conformations of biopolymers and biopolymer aggregates at the atomistic level.[65,67−69] In REMD, multiple simulations of identical systems are run concurrently at a range of temperatures and allowed to exchange with neighboring systems based on the Metropolis criterion; the technique can be thought of as a random walk in temperature space.[70] This effectively allows for stable configurations discovered by higher temperature replicas to "trickle down" to the lowest temperature replica, which enables the discovery of stable configurations even in systems characterized by inherently slow configurational rearrangement. We note that REMD simulations of explicitly solvated systems require a greater number of replicas than implicitly solvated systems, but we believe the use of REMD in studies of proteins in explicit solvents is sufficiently well established to justify its use in our study.[71−74]

In this investigation, we use REMD to reveal the equilibrium configurations of a solution of a model EPS on length scales up to 10 nm as a function of water content and cross-linking cation (Ca or Na). We posit that 10 nm scale simulations, while inherently incapable of representing EPS heterogeneity on larger length scales, can provide insight on key molecular level processes and energetics that enable the persistence of microdomains and other larger scale properties. For simplicity, we restrict our focus to solutions of the polyanionic polysaccharide alginate. Alginate was chosen because of its widespread use in experiments and simulations as a simple model of biofilms and the gel foulant layers of water treatment membranes.[9,75−80] In nature, alginate exists as a copolymer with repeating units of the stereoisomers α-D-mannuronate (M) and β-L-guluronate (G), which are carboxylated hexopyranoses.[81] Repeating units of the G monomer are known to form stable cross-linkages with calcium ions via the "egg-box model".[82−88] This model results in condensed lateral associations of alginate in which the number of monomer units between cross-linkages actually increases with increasing calcium concentrations (the opposite of covalently cross-linked gels).[89] For simplicity and to avoid condensed systems resulting from the polyG−Ca^{2+} interactions, we model alginate as repeating M units, which form milder electrostatic interchain associations through Ca^{2+} between the negatively charged carboxylate groups (COO^-). We take advantage of this to readily tune attractive alginate−alginate interactions by varying the ratio of Na^+ to Ca^{2+}.

A relatively limited number of previous MD simulation studies have examined the structure of solutions of alginate or other EPS constituents. Plazinski[90] and Plazinski and Drach[83] investigated the nature of the Ca^{2+}-mediated linkages between alginate strands in an explicit aqueous solvent, but these

https://doi.org/10.1021/acs.jpcb.2c07129
J. Phys. Chem. B 2023, 127, 1828−1841

studies limited the size of their system to two oligomers. Hecht and Srebnik[91] used a tempering technique to shed light on the structures of longer chains (N = 20) as a function of M/G content, but this study used an implicitly modeled solvent and, therefore, could not provide information on the role of water in structure formation or on the dynamics of water in the simulated structures. Here, we use the REMD simulation methodology to discover equilibrium configurations in comparatively large systems despite the slow rearrangement kinetics of the polymer matrix. Simultaneously, we use a fully explicit water model to establish how these structures might exist in thermodynamic equilibrium with various aqueous environments, notably through determination of the water excess chemical potential in simulated gel microstructures. Ultimately, the resulting simulations provide the first glimpse—to the best of our knowledge—of the equilibrium atomic-level configurations within a polysaccharide gel on length scales up to 10 nm as a function of water content and cation identity. Through an exploration of the thermodynamic basis for this structure, we show that distinct water energetics within the gel may play a key role in the structural coherence and desiccation resistance conferred by the EPS matrix.

Finally, we note that although the present work focuses on pure alginate gels with a simplified structure (only M isomers, no other EPS components) and aqueous chemistry (only Na or Ca ions), the insights generated through our simulations should be relevant to a variety of biological and engineered systems. The microstructure of the biofilm matrix is foundational not only to the lives of its inhabiting microorganisms but also to the ecosystem in which the biofilm exists, whether it be the ocean,[92,93] the rhizosphere,[94] a water treatment facility,[95−98] or the lung of a cystic fibrosis patient.[99,100] Simultaneously, beyond their importance as a component of many biofilms, pure alginate gels have important applications in drug delivery,[101,102] wound healing,[103] water harvesting,[104] and membrane separation technologies.[105,106] Lastly, our results also have the potential to deepen the understanding of the biological roles of analogous charged polysaccharides, e.g., mucopolysaccharides in the glycocalyx that surrounds epithelial cells.[107,108]

METHODS

Simulated Systems. REMD was used to discover equilibrium configurations of alginate gels for 21 different systems with identical alginate contents but with different Ca−Na ratios (with 0, 50, or 100% of alginate anionic charge balanced by Ca vs Na) and water contents (65, 70, 75, 80, 85, 90, or 95% by weight). Each of the systems consisted of 10 strands of alginate polymers with 20 monomers each (mass of 3.44 kDa) interspersed in a solution of explicitly modeled water molecules. All counterions balance the charge of the alginate polyanions, and our simulations therefore mimic zero-salinity conditions regardless of water content. The length of the alginate strands was limited to a value roughly 100 times shorter than that observed in bacterial biofilm gels[109] to minimize the likelihood of self-interaction between periodic images of the same molecule. The lowest water content was set to 65% because the dehydration process from 70 to 65% water resulted in cavitation of the solvating water in the Na− and Ca−Na-balanced gels. The Ca-balanced gels were able to withstand cavitation at these dehydration levels, presumably because of the tighter condensation of alginate strands.

MD simulations were performed using the GROMACS 2021.2 package.[110] van der Waals and electrostatic interactions were calculated with a cutoff distance of 12 Å. Long-range electrostatic interactions were calculated with the particle−particle−particle−mesh method of Hockney and Eastwood.[111] All hydrogen bonds in the simulation were constrained using the LINCS algorithm.[112] Interatomic interactions were described using the SPC/E model[113] for water molecules and the revised GROMOS56a6_Carbo force field[114] for alginate polymers. The carboxylate groups on each alginate monomer were parameterized according to Project et al.,[115] as in Plazinski and Drach.[83] Sodium and calcium ions were parameterized with the GROMOS 53a6 force field.[116] We note that the predictions of MD simulations are sensitive to the choice of inter-atomic potential models and that although the combination of force fields used in this study has been extensively validated,[117−120] their accuracy in the modeling of polysaccharide gels is still under evaluation.[121,122] As a partial validation of the alginate model used in our simulations, we calculated the persistence length of an identically parameterized 60-mer (see Figure S11). Our simulation methodology yielded a persistence length of 15.9 ± 0.04 nm, which is within the range of 12−16 nm observed in previous experimental and computational investigations.[123] In addition, we calculated calcium-water and calcium-carboxylate radial distribution functions (RDFs), as reported in the Supporting Information (Figure S12) to verify that the local coordination of calcium ions as important alginate cross-linkers was consistent with that reported in previous simulation studies.[86,90] All carboxylate groups were modeled in their deprotonated form, as expected under near neutral pH conditions. We used three different counterion environments to charge balance the alginate strands: 200 sodium ions; 100 calcium ions; and a mixture of 100 sodium ions and 50 calcium ions. The methods of dehydration and equilibration were identical for the three ionic environments.

Generation of Equilibrated Configurations. The initialization of the three ionic environments involved the following procedure. First, a single alginate strand was equilibrated with sodium ions and water molecules in a 10 × 10 × 10 nm simulation cell. Next, 10 replicates of the equilibrated alginate strand and counterions were randomly packed[124] with a minimum center of mass separation of 15 Å in a 15 × 15 × 15 nm simulation cell with periodic boundaries and solvated with water molecules. This resulted in an initial water mass content of 99%. Each of the three systems underwent an initial equilibration in the *NPT* ensemble for 10 ns and then, dehydration to 97% water content by mass. The dehydration procedure involved deleting a random selection of water molecules that constituted 5% of the total number of water molecules and then running *NPT* equilibration for 1 ns. These two steps were repeated until the water content reached the desired level. The 97% water content systems then underwent a 50 ns REMD equilibration, and the lowest temperature replica was dehydrated to 95%, which then underwent further REMD equilibration. This process of dehydration, followed by a short (1 ns) equilibration by MD simulations in the *NPT* ensemble and a longer (50 ns) equilibration using REMD, was repeated until REMD-equilibrated configurations had been obtained for each system at seven different water contents between 95 and 65%. Finally, equilibrium properties were evaluated from a 10 ns *NVT* ensemble simulation of the six lowest temperature REMD

https://doi.org/10.1021/acs.jpcb.2c07129
J. Phys. Chem. B 2023, 127, 1828−1841

structures after a further 1 ns of equilibration in the *NPT* ensemble.

The REMD methodology consisted of 100 replicas equally spaced thermally in a temperature range of 300 to 399 K. A temperature interval of 1 K resulted in an exchange probability of 20 to 40%. At a water content of 65%, fewer replicas were needed to achieve similar exchange probabilities, and thus, the number of replicas was reduced to 50 and the temperature interval increased to 2 K. During each REMD equilibration run, the replicas were first equilibrated for 100 ps in the *NVT* ensemble. Then, each of the replicas was run concurrently in the *NVT* ensemble for 50 ns and permitted to exchange with neighboring replicas every 1000 timesteps (1 ps). We verified the convergence of the REMD equilibration for all water contents. The details of this verification are presented in the Supporting Information (Figures S10 and S13).

The methodology outlined above resulted in an array of alginate gel simulations at varying levels of Ca and water content. At each set of environmental conditions, an ensemble of the six lowest temperature replicas (300 to 305 K) was taken to be representative of a gel at the corresponding calcium and water content. We note that the simulated systems are not meant to be representative of a macroscopic alginate gel with a corresponding average water content but rather give insights into the molecular architecture of 10 nm scale regions within a gel or biofilm with a corresponding water and ionic environment. Even with periodic boundaries, our simulation cell is too small to capture larger-scale heterogeneities within biofilms: as noted in the introduction, biofilms are heterogeneous structures, such that a biofilm with an overall water content of 95% might contain regions with >99% water and regions with <80% water.

Structure Characterization. The resulting configurations were first characterized in terms of their structure. The solvent accessible surface area (SASA) of the alginate was calculated using the double cubic lattice method outlined in Eisenhaber et al.[125] using a solvent particle with a radius equivalent to that of a water molecule (1.4 Å). Analogous calculations were carried out with a probe radius of 3.0 Å, i.e., considering the first hydration layer as part of the alginate framework. Final SASA values were computed from an average of values taken every picosecond over a 500 ps trajectory in the *NVT* ensemble at 300 K.

We also report the average mass-weighted radius of gyration (R_g) of the alginate strands for each of the three ionic environments as they are dehydrated. R_g values are calculated using the following formula

$$R_g = \left(\frac{\sum_i \|\boldsymbol{r}_i\|^2 m_i}{\sum_i m_i} \right)^{1/2} \tag{1}$$

where $\boldsymbol{r}_i$ is the position of atom i with respect to the center of mass of the molecule, and m_i is the mass of atom i. The radius of gyration gives a rough measure of the compactness of individual alginate strands, i.e., the volume of the configurational space occupied by the strands.

The pore size distribution (PSD) was determined by first calculating the fractional free volume (FFV, excluding the alginate) of the simulation cell using test particles with a size ranging from 0 to 4 nm. The method involves attempting 500 hypothetical insertions per nm^3 of a hard sphere with the corresponding radius. If the sphere overlaps with any alginate atom (as defined based on the atomic radii evaluated by Bondi),[126] the insertion fails and the position is considered occupied. We note that the absolute values of FFV are sensitive to the choice of atomic radii (for example, the radii compiled by Bondi are not identical to the radii implied by the interatomic potential models used here). To minimize the impact of this effect, calculated FFV values were normalized to the FFV calculated from the test insertion of a sphere with a radius of 0 nm. Insertions are attempted every picosecond of a 500 ps *NVT* run. Finally, the PSD was calculated by taking the derivative of the plot of FFV versus the test particle radius. We note that the PSDs calculated with this method (commonly used in atomistic simulation studies)[127,128] correspond to a distribution of distances to the nearest surface and not strictly to the distribution of pore sizes conventionally measured, e.g., by N_2 gas adsorption or Hg intrusion porosimetry.

Hydration Energetics. To explore the possible thermodynamic basis for the heterogeneity observed in biofilms, we set out to investigate how the enthalpy and free energy of hydration change both as a function of counterion type and water content. All quantities were taken from a simulation run in the *NVT* ensemble, and so the free energy measured is the Helmholtz free energy, $F = U - TS$, where U is the total internal energy of the system and TS the entropic component of the free energy.

The enthalpy of hydration was approximated as[129]

$$\Delta h_{\text{hydration}} = \Delta u_{\text{pot,w}} + \Delta u_{\text{pol}} - RT \tag{2}$$

where $\Delta u_{\text{pot,w}}$ is the specific potential energy of water less that of a single water molecule in vacuum, Δu_{pol} is a correction for the polarization energy not captured by the MD model, and R is the ideal gas constant. As the systems are dehydrated, the specific potential energy of water is calculated as the change in potential energy normalized by the change in water content, Δn_w

$$\Delta u_{\text{pot,w}} = \left(\frac{\partial U_{\text{pot,w}}}{\partial n_w} \right)_{N_{i\neq w},V,T} \cong \frac{\Delta U_{\text{pot}}}{\Delta n_w} \tag{3}$$

In eq 3, the term on the right side was evaluated as the slope of U_{pot} versus n_w calculated from our simulation results at different water contents. Because of the small pressure of the simulated systems, calculated values of $u_{\text{pot,w}}$ are essentially identical to the specific enthalpy of water, $h_w = u_w + P\Delta V/\Delta n_w$, where the second term on the right side is negligible ($P\Delta V/\Delta n_w \approx 0.002$ kJ mol^{-1}).

To complete the thermodynamic picture, we also determined the chemical potential of water in the gels or the differential free energy of hydration

$$\mu_w = \left(\frac{\partial F}{\partial n_w} \right)_{N_{i\neq w},V,T} \tag{4}$$

More precisely, we calculated the excess part of the chemical potential, which excludes the ideal component associated with the free energy of a single water molecule in ideal gas conditions ($\mu_w^{\text{excess}} = \mu_w - \mu_w^{\text{ideal}}$). The excess chemical potential was evaluated analytically from MD simulation trajectories based on potential distribution theory[130,131] using the Widom insertion method. This approach relies on the relation[132,133]

https://doi.org/10.1021/acs.jpcb.2c07129
J. Phys. Chem. B 2023, 127, 1828−1841

$$\mu_w^{excess} = -kT \ln\left(\left\langle \exp\left(\frac{-\Delta U_{pot,TPI}}{kT}\right)\right\rangle\right) + kT \ln\frac{\rho}{\rho_0} \quad (5)$$

where $\Delta U_{pot,TPI}$ is the change in total potential energy associated with the hypothetical addition of a single water molecule at a randomly selected location in the simulated system, and the brackets denote an average over a large number of hypothetical insertions. The second term on the right side is a correction for the volume fraction occupied by alginate, evaluated based on the ratio of the atomic density of water molecules in our simulated systems, ρ, and in bulk liquid water, ρ_0. For each of our simulated systems, we used 60,000 randomly selected insertion locations per nm^3 per ps. At each insertion location, 5000 insertions were attempted allowing the water molecule to rotate and translate within a sphere of radius 0.5 Å. Additional details on our Widom TPI analysis are presented in the Supporting Information.

In addition to the excess chemical potential, we also present the water activity $a_w = \exp(\Delta\mu/kT)$ as a measure of how the chemical potential of water in our systems differs from that of pure water. Water activity is formally defined as the ratio of the partial pressure of water in equilibrium with the system to the partial pressure of water in equilibrium with pure water. Therefore, water activity acts as a quantification of the thermodynamic driving force of water into or out of the system, relative to a hypothetical reservoir of pure liquid water.

RESULTS AND DISCUSSION

Structure of the System in Dilute Conditions. The most dilute systems analyzed in this investigation are alginate solutions with a water content of 95% by mass. As shown in Figure 1, the alginate molecules exhibit a strong preference for a linear conformation in all three systems. The elongated nature of the strands promotes the formation of structures that extend continuously in all directions through the periodic boundary conditions, such that the simulated configurations essentially reflect the inside of an alginate gel.

As shown in Figure 1a, the sodium-balanced system exhibits alginate strands that are homogeneously distributed throughout the simulation cell. In the same dilute condition, the presence of calcium ions causes a significant amount of interchain aggregation of the strands, as shown in the Na−Ca balanced system (Figure 1b) and particularly in the Ca balanced system (Figure 1c). This increasing aggregation is consistent with the expectation that Ca ions act as semi-stable bridges between COO^- groups of neighboring alginates,[30,90,134] as confirmed by visual examination of equilibrated structures. The closer coordination of Ca (vs Na) by the COO^- groups is evident in Figure 1b, where Ca ions are tightly associated with the alginate strands, whereas many Na ions are more loosely associated with the organic polyanion.

Further insights into the effect of water content on the molecular architecture of the alginate gels can be gained by examining their PSD. More precisely, Figure 1d shows the distribution of distances to the nearest alginate surface for the Na, Na−Ca, and Ca balanced systems at 95% water content. Results at lower water contents are presented in Figure S1. The dashed line shows a theoretical prediction for an ideal assemblage of parallel, hexagonally packed (i.e., maximally spaced) cylinders with a radius of 0.25 nm in a volume equivalent to the Na-alginate simulation with 95% water. As

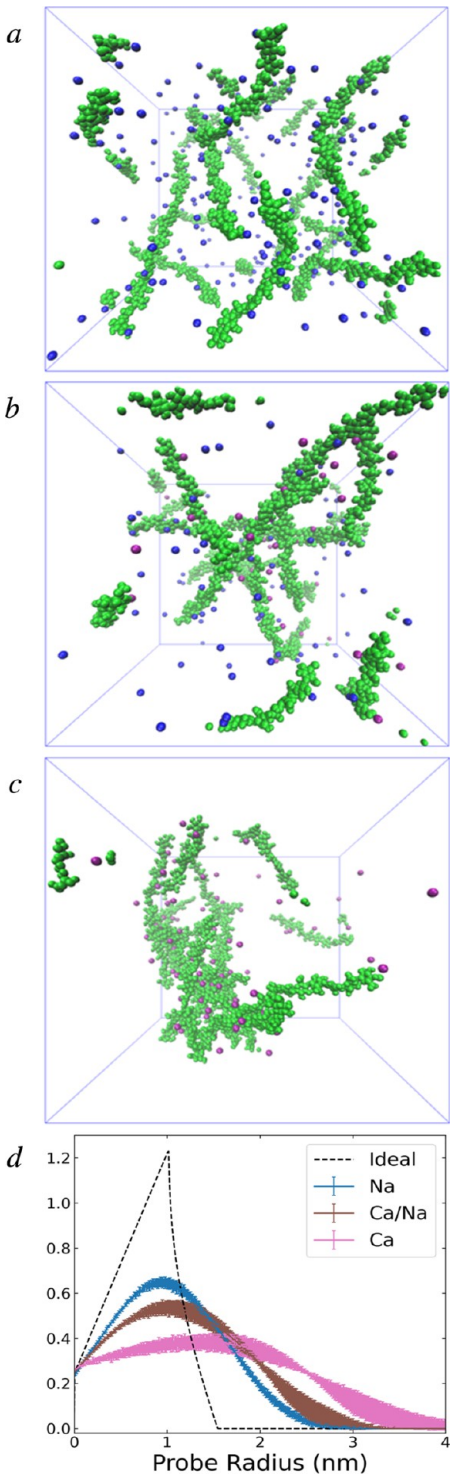

Figure 1. (a−c) Snapshots of REMD-equilibrated systems with 95% water at 300 K for alginate charge-balanced by Na, Na−Ca, or Ca ions (from top to bottom). The simulation cell width is ≈10.5 nm. Alginate strands are shown in green, Na ions in blue, and Ca ions in fuchsia. Water molecules are not shown. (d) Pore size distributions of REMD-equilibrated systems with 95% water at 300 K. The dashed line shows the relationship predicted for a system containing parallel, maximally spaced cylinders with a radius of 0.25 nm.

expected, all curves have identical values at $r = 0$, reflecting the surface area of the alginate strands as determined using a probe of radius 0. The slope of the curves at low r decreases from the idealized system to the Na, Na−Ca, and Ca balanced systems,

https://doi.org/10.1021/acs.jpcb.2c07129
J. Phys. Chem. B 2023, 127, 1828−1841

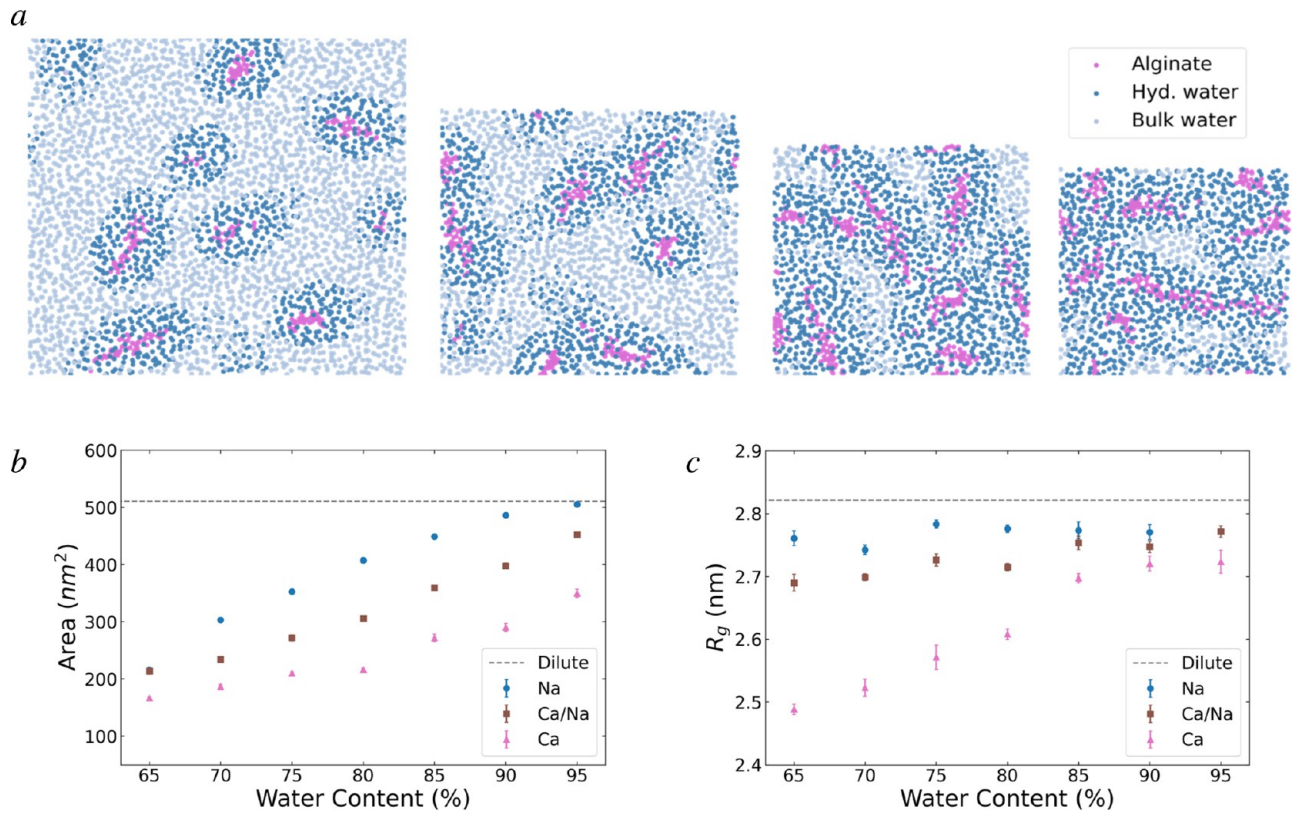

Figure 2. (a) Snapshots of a 1 nm thick cross-section of Na-alginate at water contents of 95, 90, 85, and 80% from left to right. The pink dots represent the location of alginate atoms. Dark blue dots show the center-of-mass locations of water molecules that are within two water diameters (6 Å) of an alginate strand, and light blue dots denote water molecules further than 6 Å from alginate. (b) Accessible surface area of the alginate strands as seen by a hypothetical probe with a radius equal to the diameter of a water molecule. The results quantify the interfacial area between water located within vs beyond the first hydration shell of alginate. The dotted line shows the surface area of 10 infinitely-spaced alginate strands. The error bars represent the standard error over the six lowest temperature replicas. (c) Average radius of gyration of individual alginate strands. Error bars represent the standard error over the three lowest temperature replicas. The dotted line shows the R_g value of a single alginate strand in the limit of infinite dilution.

reflecting increasing aggregation. Comparison of the different curves confirms that the Na balanced system is relatively uniform (in particular, the peak position, which roughly reflects the most likely pore radius, is identical in the Na balanced and ideal systems). In contrast, the Ca balanced system is non-uniform and exhibits a greater abundance of relatively large pores, with a peak pore radius ~2 times larger than for the Na balanced or idealized systems. We note that the scale of the heterogeneity in the Ca balanced system is likely constrained by the finite size of our simulation cell (i.e., for a 10 nm simulation cell size with 95% water, the largest observable pore radius is on the order of 4 nm), such that our simulations likely underestimate the difference in pore size distribution between Na- and Ca-alginate.

In addition to offering insight into the nature of alginate aggregation, the PSD also offers insight into the way in which water is confined in these gels. As mentioned already, previous studies indicate that water structure and dynamics are significantly impacted by the vicinity of nearby interfaces to distances of up to 1 nm.[57] Therefore, the PSD curves reported in Figure 1d reveal that in Na-alginate with 95% water content, up to half of the pore water may have properties tangibly distinct from those of bulk liquid water. In the Ca balanced system with 95% water content, the fraction of water impacted by the alginate strands is significantly lower on the order of 20% (or less if our simulations underestimate the heterogeneity of Ca alginate as suggested above).

Overall, the results presented in Figure 1 indicate that the simulation methodology developed here can generate well-equilibrated structures of alginate gels despite the expected slow conformational rearrangement of these gels. Results obtained with different aqueous chemistries show a strong influence of the Na−Ca ratio on alginate aggregation and pore size, in agreement with strong differences in mechanical properties and hydraulic permeability measured for Na versus Ca balanced alginate in previous studies.[24,25,28,29,32,135,136]

Structure of the System at Lower Water Content. As described in the Methods section, a succession of dehydration and REMD equilibration steps was used to generate molecular architectures for three ionic systems as a function of hydration level. Results are shown in Figure 2a in the case of the Na-alginate system, where the four panels show cross-sections of the simulated system at four hydration levels between 95 and 80%. As shown in Figure 2a, dehydration causes a transition to configurations where most of the pore water is located within two monolayers of the nearest alginate molecule, yet water content remains high (80%). Furthermore, even as dehydration imposes a closer arrangement of alginate strands, interactions between neighboring strands remain predominantly water-mediated as shown by the low abundance of direct alginate−alginate contacts. Note that in each dehy-

https://doi.org/10.1021/acs.jpcb.2c07129
J. Phys. Chem. B 2023, 127, 1828−1841

dration step, we decrease the percentage of water by mass in the system by a constant interval. Therefore, each successive dehydration involves the removal of fewer water molecules than the previous dehydration interval.

The progressive aggregation of alginate strands with increasing alginate mass fraction can be quantified by evaluating the progressive decrease in the SASA of the strands. Predicted values for our three simulated systems, shown in Figure S3, indicate that the SASA of the Ca-balanced system is reduced by 10 to 20% relative to the Na system. For all three ionic environments, the surface area decreases monotonically as water is removed from the system. In other words, the degree of alginate aggregation is enhanced by dehydration, and for the Na-alginate system, aggregation is only possible through dehydration. However, the decrease in SASA associated with aggregation is relatively small in all systems, as expected based on the importance of water-mediated interactions between alginate molecules noted above, i.e., even when alginate molecules aggregate, their surface remains predominantly coated with water.

As an alternative measure of the alginate surface area, we present in Figure 2b the alginate accessible surface area determined using a probe radius equal to the diameter of a water molecule. This variable essentially quantifies the accessible surface area of the *hydrated* alginate strands (i.e., with the first layer of hydration water considered a part of the alginate framework). Values lower than those calculated for isolated strands indicate overlap between the hydration waters of neighboring alginate strands. Our results show that the addition of calcium results in a significant reduction (~40%) of the hydrated surface area of the alginate polymers. This reduction is much greater than the corresponding reduction of the standard SASA (10 to 20%), which indicates that the Ca-alginate aggregates include extensive alginate−water−alginate linkages. We also note much steeper drops in the hydrated surface area as the gels are dehydrated. At 65% water content, the Na− and Ca−Na-alginate gels display a hydrated surface area 35 to 40% that of an isolated alginate strand. In other words, near the onset of cavitation in our simulated systems, about two-thirds of the alginate surface participates in alginate−alginate interactions mediated by two or fewer water layers.

An additional measure of the microstructural changes associated with dehydration is presented by the average radius of gyration (R_g) of the alginate strands, reported in Figure 2c for each of the three ionic systems as a function of water content. As shown in Figure 2c, the average R_g value in the Na-alginate gel is almost invariant with gel hydration. Similarly, the R_g value in the Ca−Na-alginate gel only decreases by about 3% as the gel is dehydrated. The lack of dependence of R_g on water content is consistent with experimental findings that R_g remains constant with increasing alginate concentrations.[123] The R_g value in Ca-alginate, however, is consistently lower than in the other two systems and decreases markedly upon dehydration, particularly at water contents below 85%, reaching a value roughly 9% lower than in the other systems in the dilute limit. Our results confirm the relative stiffness of the alginate strands observed visually in Figure 1. Our results further suggest that Ca-mediated cross-links can partly overcome this stiffness and bend the alginate molecules, whereas Na-mediated cross-links cannot. This stiffness of the alginate strands (and the partial bending required to cross-link the strands) may partly explain the limited degree of aggregation in the Na balanced system. In studies of other charged polysaccharides, increased concentrations of the polysaccharide and counterions force the counterions closer to the polysaccharide, making the chains more flexible.[137] It is reasonable to think a similar effect may occur in our simulated systems, but the magnitude of this effect is difficult to ascertain in our simulations because the simulation cell size inherently limits the length of our alginate polymers.

Additional results showing the progressive evolution of pore size distribution with dehydration in the three simulated systems are presented in Figure S1. These results indicate that the Na-balanced alginate gel retains a relatively uniform distribution during dehydration. Conversely, the two Ca-balanced systems retain a non-uniform alginate distribution during dehydration. As the alginate is progressively dehydrated, a significant peak at near-zero r values (indicating regions of the gel that have mostly expelled water) emerges at <85% water in the Ca-balanced system and at <80% water in the Na−Ca balanced system but is not observed in the Na balanced system. Qualitatively, the PSD of the Ca−Na-alginate system is more similar to that of the Na-alginate gel in the dilute limit and more similar to that of the Ca-alginate gel in the concentrated limit.

Enthalpy of Hydration. To explore the impact of molecular architecture on the thermodynamics of water in the gel, we evaluated the specific enthalpy of hydration, Δh_{hyd}, of the system as a function of ion type and water content (Figure 3a). Equivalent to the inverse of the specific enthalpy of vaporization, Δh_{hyd} is a measure of the energetic affinity of the system for water. As expected, the specific enthalpy of hydration is essentially equal to that of bulk water in the dilute limit (−43.97 kJ/mol with our simulation methodology, in agreement with values reported in experiments (−43.99 kJ/mol[138]) and in previous studies of SPC/E water (−44.08 kJ/mol[129])). Regardless of the ion type, Δh_{hyd} stays relatively constant with dehydration until the M_w/M_{alg} ratio drops below ~3, i.e., 75% water content. At water contents below 75%, Δh_{hyd} becomes abruptly more negative, indicating that water removal from the gel becomes significantly more endothermic. At this point, according to our predicted PSD curves (Figure S1), almost all the water molecules in each of the three ionic systems are part of the first hydration shell of an alginate polymer. The significant drop in the enthalpy of hydration below this water content indicates that water molecules in the first hydration layer of alginate have a more favorable enthalpy than water molecules in bulk liquid water. If we assume that the enthalpy of water−alginate interactions remains relatively constant, these results indicate that the strength of water−water hydrogen bonds beyond the first hydration layer is essentially identical to that observed in bulk liquid water, even in relatively highly dehydrated gels. We cannot conclude this definitively, however, because the magnitude of water−alginate interactions likely varies with dehydration.

Chemical Potential of Water. To understand how the molecular morphology of alginate polymers might impact larger-scale cohesion and desiccation resistance, we determined the excess chemical potential (μ_{excess}) of water in the three simulated systems. The excess chemical potential of pure water (−28.0 ± 0.2 kJ/mol with our simulation methodology, in agreement with values reported in previous studies of SPC/E water of −26.8,[139] −27.8,[140] −26.7,[141] and −28.3 kJ/mol[142]) reflects the enthalpic favorability associated with the formation of water−water hydrogen bonds and van der Waals

https://doi.org/10.1021/acs.jpcb.2c07129
J. Phys. Chem. B 2023, 127, 1828−1841

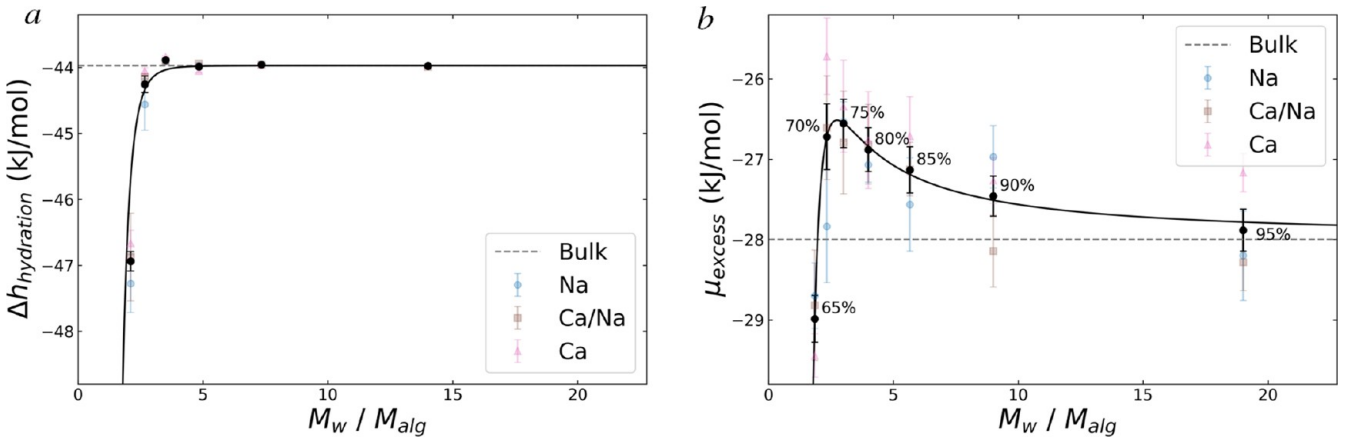

Figure 3. Plots of (a) the specific enthalpy of water (i.e., differential enthalpy of hydration) and (b) excess chemical potential of water (i.e., differential free energy of hydration) in the three gels as a function of the mass ratio of water to alginate (including counterion mass). The dotted lines show the specific enthalpy of hydration and excess chemical potential for pure SPC/E water calculated using our simulation methodology. The black dots represent the average taken over the three ionic environments (18 total μ_{excess} calculations per value of M_w/M_{alg}). The solid black lines show fitted curves of the form (a) $A(M_w/M_{alg})^{-b} + \Delta h_{hyd,bulk}$ and (b) $A(M_w/M_{alg})^{-b} + C(M_w/M_{alg})^{-d} + \mu_{excess,bulk}$ where A and $-b$ are the same for both curves, and all parameters (A, b, C, and d) were fitted to the simulation predictions in (b).

interactions (−46.7 kJ/mol without the polarization correction Δu_{pol}) and the entropic penalty associated with the decreased configurational freedom of water in the liquid phase (on the order of 16 kJ/mol). If the excess chemical potential of water in our simulated systems differs from that of bulk liquid water, then water molecules should tend to migrate toward the system with the lower chemical potential to reduce the overall free energy. Thus, by comparing the excess chemical potential of water in the alginate gel systems to the excess chemical potential of pure water, we can gain an understanding of the thermodynamic driving force toward water redistribution between alginate-rich and water-rich domains within an EPS gel or a biofilm.

As shown in Figure S7, we observe no statistical difference in the excess chemical potential of water as a function of calcium content. Therefore, in Figure 3b, we report the excess chemical potential of water averaged between our three simulated systems as a function of water content. Each black circle in Figure 3b represents an average calculated over 18 distinct 10 ns long simulations. An alternative plot of the same results expressed as the activity of water, $a_w = \exp(\Delta\mu/kT)$, where $\Delta\mu$ is the difference in the chemical potential of water between our systems and pure water, is presented in Figure S8.

The results shown in Figure 3b indicate that at water contents >70%, alginate gels exhibit a water excess chemical potential less negative than that of pure water, i.e., water in the gels has an activity greater than 1. This observation is consistent with the known cohesive nature of alginate gels: if water had a lower chemical potential in the gel than in pure water, alginate gels exposed to pure water would tend to swell and disaggregate. Our results also are consistent with previous theoretical studies suggesting the existence of a miscibility gap in alginate−water mixtures.[79] In addition, our prediction that $a_w > 1$ within alginate gels at water contents typical of biofilms is consistent with observations in food chemistry that water activities $a_w > 1$ are conducive to microbial life, whereas antibacterial properties start being detected in systems with $a_w < 0.94$.[143]

The invariance of the excess chemical potential with the Na/Ca ratio indicates that the presence of calcium has little to no effect on the thermodynamics of water inside the gel. This finding is unexpected in light of the strong impact of Na versus Ca on alginate aggregation and microstructure (Figure 1) but is supported by our similar observations on the enthalpy of hydration (Figure 3a). If correct, our results appear to imply that the impacts of Ca ions on biofilm properties reported in the literature[24,25,28,29,32,135,136] reflect either a difference in mechanics (for example, a higher yield stress of Ca alginate associated with stronger cross-linking of alginate strands or a high permeability associated with the existence of large pores in Ca alginate) or, alternatively, the existence of driving forces that are not captured at the ∼10 nm scale of our simulated systems. With regard to this last point, the aforementioned possibility that our simulations underestimate the abundance of large pores (filled with bulk-liquid-like water) in Ca-alginate implies a possible bias in the magnitude (but not in the sign) of the thermodynamic driving force toward hydration or dehydration.

In Figure 3, we report the best-fitting curves $\Delta h_{hyd} = A(M_w/M_{alg})^{-b} + \Delta h_{hyd,bulk}$ and $\mu_{excess} = A(M_w/M_{alg})^{-b} + C(M_w/M_{alg})^{-d} + \mu_{excess,bulk}$, where A and b are identical for both curves. This choice of parametric relation is arbitrary but informed by theoretical predictions that disjoining pressure in fluid-filled slit-shaped pores between solid surfaces includes components that scale with pore width to the power of −1, −2, or −3.[144−147] The four parameters were determined by fitting the average μ_{excess} values in Figure 3b using the non-linear least squares method. The coefficient and exponent of the first term were found to accurately represent the Δh_{hyd} values in Figure 3a. The best-fitting values of b and d are 6.4 and 1.1, respectively.

The fits shown in Figure 3 further illustrate the relationship between the differential enthalpy of hydration and the excess chemical potential (i.e. the differential free energy of hydration). Specifically, the results shown in the two curves are related through

$$\mu_{excess} = \Delta f_{hyd} = \Delta h_{hyd} - T\Delta s_{hyd} \quad (6)$$

https://doi.org/10.1021/acs.jpcb.2c07129
J. Phys. Chem. B 2023, 127, 1828−1841

where Δf_{hyd} and Δs_{hyd} are the differential free energy and entropy of hydration, respectively. Thus, our results indicate a $-T\Delta s_{hyd}$ term that is positive and proportional to $(M_w/M_{alg})^{-1.1}$. In other words, the differential entropy of hydration is always negative, indicating that it is entropically unfavorable to transfer a water molecule to the system from a hypothetical reservoir of pure liquid water. Furthermore, this entropic penalty increases as the gels are dehydrated. Our results are consistent with the fact that as the gels are dehydrated, the hydrating water phase becomes increasingly confined by the alginate matrix, which appears to limit the configurational space accessible to the water molecules. This confining effect of the alginate matrix on the chemical potential of water in the gels seems to be associated with the polymeric nature of the alginate molecules: in similar MD simulations of mono and polysaccharide solutions,[148] the chemical potential of water decreased monotonically with increasing organic concentration and degree of polymerization. We note that previous studies reveal a relatively high sensitivity of water activity predictions in organic solutions to the choice of interatomic potential parameters.[148] Therefore, the magnitude of the entropic term identified here should be taken with caution.

CONCLUSIONS AND IMPLICATIONS FOR THE BIOFILM MATRIX

The results presented above have notable implications for our understanding of the biofilm matrix. First, they indicate that the thermodynamics of water in alginate gels with > 65% water tend to favor a phase separation between an alginate-rich phase and a water-rich phase, regardless of the identity of the counterbalancing ion. This is consistent with the cohesive nature of alginate gels and with the persistence of sharp density gradients within the biofilm matrix.[15] It also is consistent with experimental observations that dehydrated biofilms, when exposed to bulk liquid water, spontaneously rehydrate only up to water contents on the order of ∼70% as shown, e.g., in experiments with a *B. subtilis* mutant that produces EPS but not the main biofilm protein (Δ*tasA* strain) by Ido et al.[149]

One potential implication of our results concerns the mechanism by which EPS confers resistance to desiccation. Observations such as those that the genes responsible for alginate production in the soil bacterium *Pseudomonas putida* are turned on under water-limiting conditions[9,150,151] have classically been interpreted as indicating that desiccation resistance results from the hygroscopic nature of the biofilm matrix—its ability to absorb water from the atmosphere. Indeed, the observation that two of our simulated systems undergo cavitation at a water content between 65 and 70% indicates that these gels exhibit a strong resistance to desiccation below this level (i.e., the gel prefers to cavitate rather than collapse, likely due to the stiffness of the three-dimensional network of alginate strands).

Our results, however, also reveal a second mechanism whereby alginate may protect cells from fluctuations in water availability: high water activity within of the alginate gels (a_w > 1) suggests that EPS gels may maintain a thermodynamic driving force for water out of the extracellular space and into the cells. In addition, this driving force increases in strength as the biofilm becomes more water stressed or as the concentration of alginate in the extracellular space increases. This finding implies that cells may be able to counteract water-stressed conditions (low osmotic potential) by excreting alginate and, also, may be able to tune osmotic pressure within biofilms by controlling the balance of EPS and osmolytes.[9] This result is consistent with the observation that certain bacterial species secrete alginate in environments with little water or with a high concentration of solutes.[152]

The high activity of water in alginate gels at >70% water content may also play a role in the stabilization of extracellular molecules such as proteins and DNA, as the activity and stability of these molecules are very sensitive to changes in water activity.[153] Our results provide evidence that as a biofilm dehydrates, alginate can increase the water activity of the extracellular space, or phase separation of alginate may give rise to regions of high water content that could prolong the stability and activity of extracellular biopolymers essential to biofilm viability. Indeed, Svenningsen et al.[22] found that turning off the gene for alginate production in the biofilm-producing soil species *P. putida* leads to a greater buildup of ROS with desiccation. One possible explanation for this connection between ROS buildup and loss of alginate is that alginate gels prolong the activity of ROS-cleaning proteins by increasing the water activity as the biofilm is dehydrated.

The benefit of the increased chemical potential of water at low water contents to the cells is prolonged if the alginate is somehow prevented from collapsing to the low water content at which it returns to a phase equilibrium with bulk liquid water. Complete collapse of the alginate polymers in these systems may be prevented or slowed by the extended nature of the alginate strands, which is only partly captured in our simulations due to the relatively short length of our simulated polymer strands. The relative stiffness of the alginate strands (indicated by their high radius of gyration and its minimal decrease with dehydration) likely helps prevent this collapse by inhibiting the formation of close-packed arrangements.

As mentioned above, our systems provide only a nanoscale view of alginate gels and therefore do not capture polymer physics on the length scales of actual alginate polymers (>100 nm).[109] In polymer solutions, the free energy is dictated by a balance between the monomer−monomer and monomer−solvent interactions with the entropic resistance of the polymers to complete collapse and to complete extension. While our simulations capture the monomer−monomer and monomer−solvent interactions, it is unclear whether the entropic term associated with the polymers is fully captured by our calculations of the chemical potential of water. The simulated alginate strands approach the persistence length of real alginate strands and, therefore, should at least partly capture the manner in which the maximization of the configurational entropy of the polymers stretches and compresses the solvating water in a way that is captured by the Widom insertion method. However, the similarity in length between the simulation cell and individual strands may introduce artifacts, e.g., by preventing the emergence of heterogeneity on length scales similar to or larger than the simulation cell dimension. Although the microstructural and energetic trends observed in our simulations are generally consistent with expectations, the quantitative accuracy of our predicted water energetics is difficult to ascertain in the absence of experimental validation for alginate strands like those used in our study (i.e., with 20 M-monomer units). We note that the structural properties of water-organic mixtures tend to be relatively weakly sensitive to MD simulation

https://doi.org/10.1021/acs.jpcb.2c07129
J. Phys. Chem. B 2023, 127, 1828−1841

methodology, while their energetic properties tend to be much more sensitive.[148]

Unfortunately, the simulations become highly computationally expensive at water contents above 95%. However, the trend in the excess chemical potential of water in all three gels suggests that at high water contents, they approach the excess chemical potential of pure water. This indicates that regions of high and low alginate concentrations can co-exist in thermodynamic equilibrium, in agreement with thermodynamic predictions.[79] This is a significant finding for understanding the macroscale stability of the biofilm matrix, as it suggests a way in which the connectivity of the polymer network might be preserved across water-rich regions. All in all, our results are consistent with the experimental findings of a non-monotonic dependence of biofilm mechanical stability and permeability on the calcium content. At low Ca contents, the connectivity of the polymer network is strengthened by the formation of high-energy cross-links between alginate polymers.

The predicted thermodynamic tendency toward the phase separation of the polymer solution into polymer-rich and water-rich regions is reminiscent of the coacervation process in biological systems that has gained significant attention in the past two decades.[154,155] The formation of coacervates, the polymer-rich phase, is driven by the electrostatic attractions of polyelectrolytes with oppositely charged polymers or with inorganic counterions. The theory of coacervation is similar to traditional polymer scaling theory except that in the former, the species are in chemical equilibrium with the solvent as opposed to thermal equilibrium in the latter.[155] Theories of coacervation largely consider the solvating water as a continuum and thus have not explored the possibility of water as a phase separating actor itself.[155] Here, by examining the chemical potential of water in the alginate solution, we have observed a yet unexplored driving force for coacervation, namely, an increase in the chemical potential of water at intermediate regimes of polymer concentration. In our opinion, these findings call for greater attention to water's identity as a phase separating actor as opposed to treating it simply as the medium in which phase separation occurs.

■ ASSOCIATED CONTENT

Supporting Information

The Supporting Information is available free of charge at https://pubs.acs.org/doi/10.1021/acs.jpcb.2c07129.

> Additional simulation details including validation of the REMD methodology and the alginate force field parameters; further details on structure and thermodynamic analysis; and additional results: pore size distributions of all 18 equilibrated configurations, water mole fraction in the pore space, alginate persistence length, and calcium-alginate RDFs (PDF)

■ AUTHOR INFORMATION

Corresponding Author

Avery A. Agles − *Department of Chemical and Biological Engineering, Princeton University, Princeton, New Jersey 08544, United States;* orcid.org/0000-0001-9443-3365; Email: aagles@princeton.edu

Author

Ian C. Bourg − *Department of Civil and Environmental Engineering and High Meadows Environmental Institute, Princeton University, Princeton, New Jersey 08544, United States;* orcid.org/0000-0002-5265-7229

Complete contact information is available at: https://pubs.acs.org/10.1021/acs.jpcb.2c07129

Author Contributions

A.A.A. designed the research, carried out the simulations, analyzed the results, and wrote the initial manuscript. I.C.B. provided input on the research design and on the manuscript.

Notes

The authors declare no competing financial interest.

■ ACKNOWLEDGMENTS

This research was supported by the U.S. Department of Energy, Geosciences Program, under Award DE-SC0018419 and by the U.S. National Science Foundation under grant no. CBET 1931611. Molecular dynamics simulations were performed using resources of the Princeton Institute for Computational Science and Engineering (PICSciE) and of the National Energy Research Scientific Computing Center (NERSC), which is supported by the US Department of Energy, Office of Science, under award DE-AC02-05CH11231.

■ REFERENCES

(1) Flemming, H. C.; Wingender, J.; Szewzyk, U.; Steinberg, P.; Rice, S. A.; Kjelleberg, S. Biofilms: An Emergent Form of Bacterial Life. *Nat. Rev. Microbiol.* **2016**, *14*, 563−575.

(2) Flemming, H. C.; Wingender, J. The Biofilm Matrix. *Nat. Rev. Microbiol.* **2010**, *8*, 623−633.

(3) Vert, M.; Doi, Y.; Hellwich, K.-H.; Hess, M.; Hodge, P.; Kubisa, P.; Rinaudo, M.; Schué, F. Terminology for Biorelated Polymers and Applications (IUPAC Recommendations 2012). *Pure Appl. Chem.* **2012**, *84*, 377−410.

(4) Seviour, T.; Derlon, N.; Dueholm, M. S.; Flemming, H. C.; Girbal-Neuhauser, E.; Horn, H.; Kjelleberg, S.; van Loosdrecht, M. C. M.; Lotti, T.; Malpei, M. F.; Nerenberg, R.; Neu, T. R.; Paul, E.; Yu, H.; Lin, Y. Extracellular Polymeric Substances of Biofilms: Suffering from an Identity Crisis. *Water Res.* **2019**, *151*, 1−7.

(5) Berman, T.; Mizrahi, R.; Dosoretz, C. G. Transparent Exopolymer Particles (TEP): A Critical Factor in Aquatic Biofilm Initiation and Fouling on Filtration Membranes. *Desalination* **2011**, *276*, 184−190.

(6) Wang, R.; Hartel, R. W. Effects of Moisture Content and Saccharide Distribution on the Stickiness of Syrups. *J. Food Eng.* **2020**, *284*, 110067.

(7) Bar-Zeev, E.; Berman-Frank, I.; Girshevitz, O.; Berman, T. Revised Paradigm of Aquatic Biofilm Formation Facilitated by Microgel Transparent Exopolymer Particles. *Proc. Natl. Acad. Sci. U.S.A.* **2012**, *109*, 9119−9124.

(8) Sutherland, I. W. Biofilm Exopolysaccharides: A Strong and Sticky Framework. *Microbiology* **2001**, *147*, 3−9.

(9) Chang, W. S.; van de Mortel, M.; Nielsen, L.; Nino de Guzman, G. N.; Li, X.; Halverson, L. J. Alginate Production by Pseudomonas Putida Creates a Hydrated Microenvironment and Contributes to Biofilm Architecture and Stress Tolerance under Water-Limiting Conditions. *J. Bacteriol.* **2007**, *189*, 8290−8299.

(10) Ghafoor, A.; Hay, I. D.; Rehm, B. H. A. Role of Exopolysaccharides in Pseudomonas Aeruginosa Biofilm Formation and Architecture. *Appl. Environ. Microbiol.* **2011**, *77*, 5238−5246.

(11) Steele, D. J.; Franklin, D. J.; Underwood, G. J. C. Protection of Cells from Salinity Stress by Extracellular Polymeric Substances in Diatom Biofilms. *Biofouling* **2014**, *30*, 987−998.

(12) Morris, J. J.; Lenski, R. E.; Zinser, E. R. The Black Queen Hypothesis: Evolution of Dependencies through Adaptive Gene Loss. *mBio* **2012**, *3*, e00036-12.
(13) West, S. A.; Cooper, G. A. Division of Labour in Microorganisms: An Evolutionary Perspective. *Nat. Rev. Microbiol.* **2016**, *14*, 716−723.
(14) Dragoš, A.; Kiesewalter, H.; Martin, M.; Hsu, C. Y.; Hartmann, R.; Wechsler, T.; Eriksen, C.; Brix, S.; Drescher, K.; Stanley-Wall, N.; Kümmerli, R.; Kovács, Á. T. Division of Labor during Biofilm Matrix Production. *Curr. Biol.* **2018**, *28*, 1903−1913.
(15) Decho, A. Exopolymer Microdomains as a Structuring Agent for Heterogeneity Within Microbial Biofilms. *Microbial Sediments*; Springer, 2000.
(16) Lawrence, J. R.; Swerhone, G. D. W.; Leppard, G. G.; Araki, T.; Zhang, X.; West, M. M.; Hitchcock, A. P. Scanning Transmission X-Ray, Laser Scanning, and Transmission Electron Microscopy Mapping of the Exopolymeric Matrix of Microbial Biofilms. *Appl. Environ. Microbiol.* **2003**, *69*, 5543−5554.
(17) Costerton, J. W.; Lewandowski, Z.; Caldwell, D. E.; Korber, D. R.; Lappin-Scott, H. M. Microbial Biofilms. *Annu. Rev. Microbiol.* **1995**, *49*, 711−745.
(18) Quan, K.; Hou, J.; Zhang, Z.; Ren, Y.; Peterson, B. W.; Flemming, H. C.; Mayer, C.; Busscher, H. J.; van der Mei, H. C. Water in Bacterial Biofilms: Pores and Channels, Storage and Transport Functions. *Crit. Rev. Microbiol.* **2022**, *48*, 283−302.
(19) Ghosh, P.; Mondal, J.; Ben-Jacob, E.; Levine, H. Mechanically-Driven Phase Separation in a Growing Bacterial Colony. *Proc. Natl. Acad. Sci. U.S.A.* **2015**, *112*, E2166−E2173.
(20) Dorken, G.; Ferguson, G. P.; French, C. E.; Poon, W. C. K. Aggregation by Depletion Attraction in Cultures of Bacteria Producing Exopolysaccharide. *J. R. Soc., Interface* **2012**, *9*, 3490−3502.
(21) Schwarz-Linek, J.; Dorken, G.; Winkler, A.; Wilson, L. G.; Pham, N. T.; French, C. E.; Schilling, T.; Poon, W. C. K. Polymer-Induced Phase Separation in Suspensions of Bacteria. *EPL* **2010**, *89*, 68003.
(22) Svenningsen, N. B.; Martínez-García, E.; Nicolaisen, M. H.; de Lorenzo, V.; Nybroe, O. The Biofilm Matrix Polysaccharides Cellulose and Alginate Both Protect Pseudomonas Putida Mt-2 against Reactive Oxygen Species Generated under Matric Stress and Copper Exposure. *Microbiology* **2018**, *164*, 883−888.
(23) Mayer, C.; Moritz, R.; Kirschner, C.; Borchard, W.; Maibaum, R.; Wingender, J.; Flemming, H. C. The Role of Intermolecular Interactions: Studies on Model Systems for Bacterial Biofilms. *Int. J. Biol. Macromol.* **1999**, *26*, 3−16.
(24) Ren, T. T.; Liu, L.; Sheng, G. P.; Liu, X. W.; Yu, H. Q.; Zhang, M. C.; Zhu, J. R. Calcium Spatial Distribution in Aerobic Granules and Its Effects on Granule Structure, Strength and Bioactivity. *Water Res.* **2008**, *42*, 3343−3352.
(25) Körstgens, V.; Flemming, H. C.; Wingender, J.; Borchard, W. Influence of Calcium Ions on the Mechanical Properties of a Model Biofilm of Mucoid Pseudomonas Aeruginosa. *Water Sci. Technol.* **2001**, *43*, 49−57.
(26) Zhang, M.; Lin, H.; Shen, L.; Liao, B. Q.; Wu, X.; Li, R. Effect of Calcium Ions on Fouling Properties of Alginate Solution and Its Mechanisms. *J. Membr. Sci.* **2017**, *525*, 320−329.
(27) Barka, E.; Papayannis, D. K.; Kolettis, T. M.; Agathopoulos, S. Optimization of Ca2+ Content in Alginate Hydrogel Injected in Myocardium. *J. Biomed. Mater. Res., Part B* **2019**, *107*, 223−231.
(28) Zhang, M.; Lin, H.; Shen, L.; Liao, B. Q.; Wu, X.; Li, R. Effect of Calcium Ions on Fouling Properties of Alginate Solution and Its Mechanisms. *J. Membr. Sci.* **2017**, *525*, 320−329.
(29) You, X.; Teng, J.; Chen, Y.; Long, Y.; Yu, G.; Shen, L.; Lin, H. New Insights into Membrane Fouling by Alginate: Impacts of Ionic Strength in Presence of Calcium Ions. *Chemosphere* **2020**, *246*, 125801.
(30) Wloka, M.; Rehage, H.; Flemming, H. C.; Wingender, J. Rheological Properties of Viscoelastic Biofilm Extracellular Polymeric Substances and Comparison to the Behavior of Calcium Alginate Gels. *Colloid Polym. Sci.* **2004**, *282*, 1067−1076.
(31) Sarkisova, S.; Patrauchan, M. A.; Berglund, D.; Nivens, D. E.; Franklin, M. J. Calcium-Induced Virulence Factors Associated with the Extracellular Matrix of Mucoid Pseudomonas Aeruginosa Biofilms. *J. Bacteriol.* **2005**, *187*, 4327−4337.
(32) Jacobs, H. M.; O'Neal, L.; Lopatto, E.; Wozniak, D. J.; Bjarnsholt, T.; Parsek, M. R. Mucoid Pseudomonas Aeruginosa Can Produce Calcium-Gelled BioFiLms Independent of the Matrix Components Psl and CdrA. *J. Bacteriol.* **2022**, *204*, e0056821.
(33) Gloag, E. S.; Fabbri, S.; Wozniak, D. J.; Stoodley, P. Biofilm Mechanics: Implications in Infection and Survival. *Biofilm* **2020**, *2*, 100017.
(34) Boudarel, H.; Mathias, J. D.; Blaysat, B.; Grédiac, M. Toward Standardized Mechanical Characterization of Microbial Biofilms: Analysis and Critical Review. *npj Biofilms Microbiomes* **2018**, *4*, 17.
(35) Charlton, S. G. V.; White, M. A.; Jana, S.; Eland, L. E.; Jayathilake, P. G.; Burgess, J. G.; Chen, J.; Wipat, A.; Curtis, T. P. Regulating, Measuring, and Modeling the Viscoelasticity of Bacterial Biofilms. *J. Bacteriol.* **2019**, *201*, No. e00101-19.
(36) Gordon, V. D.; Davis-Fields, M.; Kovach, K.; Rodesney, C. A. Biofilms and Mechanics: A Review of Experimental Techniques and Findings. *J. Phys. D: Appl. Phys.* **2017**, *50*, 223002.
(37) Kučerka, N.; Papp-Szabo, E.; Nieh, M. P.; Harroun, T. A.; Schooling, S. R.; Pencer, J.; Nicholson, E. A.; Beveridge, T. J.; Katsaras, J. Effect of Cations on the Structure of Bilayers Formed by Lipopolysaccharides Isolated from Pseudomonas Aeruginosa PAO1. *J. Phys. Chem. B* **2008**, *112*, 8057−8062.
(38) Desmond, P.; Huisman, K. T.; Sanawar, H.; Farhat, N. M.; Traber, J.; Fridjonsson, E. O.; Johns, M. L.; Flemming, H. C.; Picioreanu, C.; Vrouwenvelder, J. S. Controlling the Hydraulic Resistance of Membrane Biofilms by Engineering Biofilm Physical Structure. *Water Res.* **2022**, *210*, 118031.
(39) Billings, N.; Birjiniuk, A.; Samad, T. S.; Doyle, P. S.; Ribbeck, K. Material properties of biofilms—a review of methods for understanding permeability and mechanics. *Rep. Prog. Phys.* **2015**, *78*, 036601.
(40) Even, C.; Marlière, C.; Ghigo, J. M.; Allain, J. M.; Marcellan, A.; Raspaud, E. Recent Advances in Studying Single Bacteria and Biofilm Mechanics. *Adv. Colloid Interface Sci.* **2017**, *247*, 573−588.
(41) Mattei, M. R.; Frunzo, L.; D'Acunto, B.; Pechaud, Y.; Pirozzi, F.; Esposito, G. Continuum and Discrete Approach in Modeling Biofilm Development and Structure: A Review. *J. Math. Biol.* **2018**, *76*, 945−1003.
(42) Hunter, R. C.; Beveridge, T. J. High-Resolution Visualization of Pseudomonas Aeruginosa PAO1 Biofilms by Freeze-Substitution Transmission Electron Microscopy. *J. Bacteriol.* **2005**, *187*, 7619−7630.
(43) Wu, Y.; Liang, J.; Rensing, K.; Chou, T. M.; Libera, M. Extracellular Matrix Reorganization during Cryo Preparation for Scanning Electron Microscope Imaging of Staphylococcus Aureus Biofilms. *Microsc. Microanal.* **2014**, *20*, 1348−1355.
(44) Kudlay, A. N.; Erukhimovich, I. Y.; Khokhlov, A. R. Microphase Separation in Weakly Charged Annealed Gels and Associating Polyelectrolyte Solutions. *Macromolecules* **2000**, *33*, 5644−5654.
(45) Potemkin, I. I.; Andreenko, S. A.; Khokhlov, A. R. Associating Polyelectrolyte Solutions: Normal and Anomalous Reversible Gelation. *J. Chem. Phys.* **2001**, *115*, 4862−4872.
(46) Mawatari, K.; Isogai, K.; Morikawa, K.; Ushiyama, H.; Kitamori, T. Isotope Effect in the Liquid Properties of Water Confined in 100 Nm Nanofluidic Channels. *J. Phys. Chem. B* **2021**, *125*, 3178−3183.
(47) Tambach, T. J.; Hensen, E. J. M.; Smit, B. Molecular Simulations of Swelling Clay Minerals. *J. Phys. Chem. B* **2004**, *108*, 7586−7596.
(48) Collin, M.; Gin, S.; Dazas, B.; Mahadevan, T.; Du, J.; Bourg, I. C. Molecular Dynamics Simulations of Water Structure and Diffusion in a 1 Nm Diameter Silica Nanopore as a Function of Surface Charge and Alkali Metal Counterion Identity. *J. Phys. Chem. C* **2018**, *122*, 17764−17776.

https://doi.org/10.1021/acs.jpcb.2c07129
J. Phys. Chem. B 2023, 127, 1828−1841

(49) Bourg, I. C.; Steefel, C. I. Molecular Dynamics Simulations of Water Structure and Diffusion in Silica Nanopores. *J. Phys. Chem. C* **2012**, *116*, 11556−11564.
(50) Fayer, M. D. Dynamics of Water Interacting with Interfaces, Molecules, and Ions. *Acc. Chem. Res.* **2012**, *45*, 3−14.
(51) Liu, J.; Fan, J.; Tang, M.; Cen, M.; Yan, J.; Liu, Z.; Zhou, W. Water Diffusion Behaviors and Transportation Properties in Transmembrane Cyclic Hexa-, Octa- and Decapeptide Nanotubes. *J. Phys. Chem. B* **2010**, *114*, 12183−12192.
(52) Shinyashiki, N.; Matsumura, Y.; Miura, N.; Yagihara, S.; Mashimo, S. Dielectric Study of Water Structure in Polymer Solution. *J. Phys. Chem.* **1994**, *98*, 13612−13615.
(53) Mancinelli, R. The Effect of Confinement on Water Structure. *J. Phys.: Condens. Matter* **2010**, *22*, 404213.
(54) Su, J.; Guo, H. Effect of Nanochannel Dimension on the Transport of Water Molecules. *J. Phys. Chem. B* **2012**, *116*, 5925−5932.
(55) Pascal, T. A.; Goddard, W. A.; Jung, Y. Entropy and the Driving Force for the Filling of Carbon Nanotubes with Water. *Proc. Natl. Acad. Sci. U.S.A.* **2011**, *108*, 11794−11798.
(56) Ball, P. Water is an active matrix of life for cell and molecular biology. *Proc. Natl. Acad. Sci. U.S.A.* **2017**, *114*, 13327−13335.
(57) Bocquet, L.; Charlaix, E. Nanofluidics, from Bulk to Interfaces. *Chem. Soc. Rev.* **2010**, *39*, 1073−1095.
(58) Karplus, M.; Petsko, G. A. Molecular Dynamics Simulations in Biology. *Nature* **1990**, *347*, 631−639.
(59) Laage, D.; Elsaesser, T.; Hynes, J. T. Water Dynamics in the Hydration Shells of Biomolecules. *Chem. Rev.* **2017**, *117*, 10694−10725.
(60) Kalinichev, A. G.; Kirkpatrick, R. J. Molecular Dynamics Simulation of Cationic Complexation with Natural Organic Matter. *Eurasian J. Soil Sci.* **2007**, *58*, 909−917.
(61) Iskrenova-Tchoukova, E.; Kalinichev, A. G.; Kirkpatrick, R. J. Metal Cation Complexation with Natural Organic Matter in Aqueous Solutions: Molecular Dynamics Simulations and Potentials of Mean Force. *Langmuir* **2010**, *26*, 15909−15919.
(62) Devarajan, D.; Liang, L.; Gu, B.; Brooks, S. C.; Parks, J. M.; Smith, J. C. Molecular Dynamics Simulation of the Structures, Dynamics, and Aggregation of Dissolved Organic Matter. *Environ. Sci. Technol.* **2020**, *54*, 13527−13537.
(63) Takada, S. Coarse-Grained Molecular Simulations of Large Biomolecules. *Curr. Opin. Struct. Biol.* **2012**, *22*, 130−137.
(64) Hoda, N.; Larson, R. G. Explicit- and Implicit-Solvent Molecular Dynamics Simulations of Complex Formation between Polycations and Polyanions. *Macromolecules* **2009**, *42*, 8851−8863.
(65) Bernardi, R. C.; Melo, M. C. R.; Schulten, K. Enhanced Sampling Techniques in Molecular Dynamics Simulations of Biological Systems. *Biochim. Biophys. Acta, Gen. Subj.* **2015**, *1850*, 872−877.
(66) Scott, S. E.; Fernandez, J. P.; Hadad, C. M.; MacKay, A. A. Molecular Docking as a Tool to Examine Organic Cation Sorption to Organic Matter. *Environ. Sci. Technol.* **2022**, *56*, 951−961.
(67) Abrams, C.; Bussi, G. Enhanced Sampling in Molecular Dynamics Using Metadynamics, Replica-Exchange, and Temperature-Acceleration. *Entropy* **2014**, *16*, 163−199.
(68) Kloczowkski, A. *Computer Simulations of Aggregation of Proteins and Peptides*; Humana Press, 2022; Vol. *2340*.
(69) Jang, S.; Yuan, J. M.; Shin, J.; Measey, T. J.; Schweitzer-Stenner, R.; Li, F. Y. Energy Landscapes Associated with the Self-Aggregation of an Alanine-Based Oligopeptide (AAKA)4. *J. Phys. Chem. B* **2009**, *113*, 6054−6061.
(70) Zhou, R. Replica Exchange Molecular Dynamics Method for Protein Folding Simulation. *Methods Mol. Biol.* **1999**, *350*, 205−223.
(71) Periole, X.; Mark, A. E. Convergence and Sampling Efficiency in Replica Exchange Simulations of Peptide Folding in Explicit Solvent. *J. Chem. Phys.* **2007**, *126*, 014903.
(72) Zhou, R. Free Energy Landscape of Protein Folding in Water: Explicit vs. Implicit Solvent. *Proteins: Struct., Funct., Genet.* **2003**, *53*, 148−161.
(73) Zhou, R.; Berne, B. J. Can a continuum solvent model reproduce the free energy landscape of a β-hairpin folding in water? *Proc. Natl. Acad. Sci. U.S.A.* **2002**, *99*, 12777−12782.
(74) Nymeyer, H.; García, A. E. Simulation of the folding equilibrium of α-helical peptides: A comparison of the generalized Born approximation with explicit solvent. *Proc. Natl. Acad. Sci. U.S.A.* **2003**, *100*, 13934−13939.
(75) Ang, W. S.; Lee, S.; Elimelech, M. Chemical and Physical Aspects of Cleaning of Organic-Fouled Reverse Osmosis Membranes. *J. Membr. Sci.* **2006**, *272*, 198−210.
(76) Xin, Y.; Bligh, M. W.; Kinsela, A. S.; Wang, Y.; David Waite, T. D. Calcium-Mediated Polysaccharide Gel Formation and Breakage: Impact on Membrane Foulant Hydraulic Properties. *J. Membr. Sci.* **2015**, *475*, 395−405.
(77) Barnes, R. J.; Bandi, R. R.; Chua, F.; Low, J. H.; Aung, T.; Barraud, N.; Fane, A. G.; Kjelleberg, S.; Rice, S. A. The Roles of Pseudomonas Aeruginosa Extracellular Polysaccharides in Biofouling of Reverse Osmosis Membranes and Nitric Oxide Induced Dispersal. *J. Membr. Sci.* **2014**, *466*, 161−172.
(78) Ye, Y.; Le Clech, P.; Chen, V.; Fane, A. G.; Jefferson, B. Fouling Mechanisms of Alginate Solutions as Model Extracellular Polymeric Substances. *Desalination* **2005**, *175*, 7−20.
(79) Borchard, W.; Kenning, A.; Kapp, A.; Mayer, C. Phase Diagram of the System Sodium Alginate/Water: A Model for Biofilms. *Int. J. Biol. Macromol.* **2005**, *35*, 247−256.
(80) Tow, E. W.; Rencken, M. M.; Lienhard, J. H. In Situ Visualization of Organic Fouling and Cleaning Mechanisms in Reverse Osmosis and Forward Osmosis. *Desalination* **2016**, *399*, 138−147.
(81) Lee, K. Y.; Mooney, D. J. Alginate: Properties and Biomedical Applications. *Prog. Polym. Sci.* **2012**, *37*, 106−126.
(82) Plazinski, W.; Rudzinski, W. Molecular modeling of Ca2+-oligo(α-l-guluronate) complexes: toward the understanding of the junction zone structure in calcium alginate gels. *Struct. Chem.* **2012**, *23*, 1409−1415.
(83) Plazinski, W.; Drach, M. The Dynamics of the Calcium-Induced Chain-Chain Association in the Polyuronate Systems. *J. Comput. Chem.* **2012**, *33*, 1709−1715.
(84) de Kerchove, A. J.; Elimelech, M. Formation of Polysaccharide Gel Layers in the Presence of Ca2+ and K+ Ions: Measurements and Mechanisms. *Biomacromolecules* **2007**, *8*, 113−121.
(85) Fang, Y.; Al-Assaf, S.; Phillips, G. O.; Nishinari, K.; Funami, T.; Williams, P. A.; Li, A. Multiple Steps and Critical Behaviors of the Binding of Calcium to Alginate. *J. Phys. Chem. B* **2007**, *111*, 2456−2462.
(86) Perić, L.; Pereira, C. S.; Pérez, S.; Hünenberger, P. H. Conformation, Dynamics and Ion-Binding Properties of Single-Chain Polyuronates: A Molecular Dynamics Study. *Mol. Simul.* **2008**, *34*, 421−446.
(87) Plazinski, W. Molecular basis of calcium binding by polyguluronate chains. Revising the egg-box model. *J. Comput. Chem.* **2011**, *32*, 2988−2995.
(88) Braccini, I.; Pérez, S. Molecular Basis of Ca2+-Induced Gelation in Alginates and Pectins: The Egg-Box Model Revisited. *Biomacromolecules* **2001**, *2*, 1089−1096.
(89) Davidovich-Pinhas, M.; Bianco-Peled, H. A Quantitative Analysis of Alginate Swelling. *Carbohydr. Polym.* **2010**, *79*, 1020−1027.
(90) Plazinski, W. Molecular Basis of Calcium Binding by Polyguluronate Chains. Revising the Egg-Box Model. *J. Comput. Chem.* **2011**, *32*, 2988−2995.
(91) Hecht, H.; Srebnik, S. Structural Characterization of Sodium Alginate and Calcium Alginate. *Biomacromolecules* **2016**, *17*, 2160−2167.
(92) Verdugo, P.; Alldredge, A. L.; Azam, F.; Kirchman, D. L.; Passow, U.; Santschi, P. H. The Oceanic Gel Phase: A Bridge in the DOM-POM Continuum. *Mar. Chem.* **2004**, *92*, 67−85.

https://doi.org/10.1021/acs.jpcb.2c07129
J. Phys. Chem. B 2023, 127, 1828−1841

(93) Verdugo, P.; Santschi, P. H. Polymer Dynamics of DOC Networks and Gel Formation in Seawater. *Deep Sea Res., Part II* **2010**, *57*, 1486−1493.
(94) Benard, P.; Zarebanadkouki, M.; Brax, M.; Kaltenbach, R.; Jerjen, I.; Marone, F.; Couradeau, E.; Felde, V. J. M. N. L.; Kaestner, A.; Carminati, A. Microhydrological Niches in Soils: How Mucilage and EPS Alter the Biophysical Properties of the Rhizosphere and Other Biological Hotspots. *Vadose Zone J.* **2019**, *18*, 1−10.
(95) Matin, A.; Khan, Z.; Zaidi, S. M. J.; Boyce, M. C. Biofouling in Reverse Osmosis Membranes for Seawater Desalination: Phenomena and Prevention. *Desalination* **2011**, *281*, 1−16.
(96) Bar-Zeev, E.; Belkin, N.; Liberman, B.; Berman-Frank, I.; Berman, T. Bioflocculation: Chemical Free, Pre-Treatment Technology for the Desalination Industry. *Water Res.* **2013**, *47*, 3093−3102.
(97) Bar-Zeev, E.; Passow, U.; Romero-Vargas Castrillón, S.; Elimelech, M. Transparent Exopolymer Particles: From Aquatic Environments and Engineered Systems to Membrane Biofouling. *Environ. Sci. Technol.* **2015**, *49*, 691−707.
(98) Lee, D. J.; Chen, Y. Y.; Show, K. Y.; Whiteley, C. G.; Tay, J. H. Advances in Aerobic Granule Formation and Granule Stability in the Course of Storage and Reactor Operation. *Biotechnol. Adv.* **2010**, *28*, 919−934.
(99) Ramsey, D. M.; Wozniak, D. J. Understanding the Control of Pseudomonas Aeruginosa Alginate Synthesis and the Prospects for Management of Chronic Infections in Cystic Fibrosis. *Mol. Microbiol.* **2005**, *56*, 309−322.
(100) Tan, J.; Rouse, S. L.; Li, D.; Pye, V. E.; Vogeley, L.; Brinth, A. R.; El Arnaout, T.; Whitney, J. C.; Howell, P. L.; Sansom, M. S. P.; Caffrey, M. A conformational landscape for alginate secretion across the outer membrane of Pseudomonas aeruginosa. *Acta Crystallogr., Sect. D: Biol. Crystallogr.* **2014**, *70*, 2054−2068.
(101) Wróblewska-Krepsztul, J.; Rydzkowski, T.; Michalska-Pożoga, I.; Thakur, V. K. Biopolymers for Biomedical and Pharmaceutical Applications: Recent Advances and Overview of Alginate Electrospinning. *Nanomaterials* **2019**, *9*, 404.
(102) Abasalizadeh, F.; Moghaddam, S. V.; Alizadeh, E.; Akbari, E.; Kashani, E.; Fazljou, S. M. B.; Torbati, M.; Akbarzadeh, A. Correction to: Alginate-based hydrogels as drug delivery vehicles in cancer treatment and their applications in wound dressing and 3D bioprinting. *J. Biol. Eng.* **2020**, *14*, 17.
(103) Varaprasad, K.; Jayaramudu, T.; Kanikireddy, V.; Toro, C.; Sadiku, E. R. Alginate-Based Composite Materials for Wound Dressing Application:A Mini Review. *Carbohydr. Polym.* **2020**, *236*, 116025.
(104) Entezari, A.; Ejeian, M.; Wang, R. Super Atmospheric Water Harvesting Hydrogel with Alginate Chains Modified with Binary Salts. *ACS Mater. Lett.* **2020**, *2*, 471−477.
(105) Zhao, J.; Zhu, Y.; He, G.; Xing, R.; Pan, F.; Jiang, Z.; Zhang, P.; Cao, X.; Wang, B. Incorporating Zwitterionic Graphene Oxides into Sodium Alginate Membrane for Efficient Water/Alcohol Separation. *ACS Appl. Mater. Interfaces* **2016**, *8*, 2097−2103.
(106) Galiano, F.; Briceño, K.; Marino, T.; Molino, A.; Christensen, K. V.; Figoli, A. Advances in Biopolymer-Based Membrane Preparation and Applications. *J. Membr. Sci.* **2018**, *564*, 562−586.
(107) Uchimido, R.; Schmidt, E. P.; Shapiro, N. I. The glycocalyx: a novel diagnostic and therapeutic target in sepsis. *Crit. Care* **2019**, *23*, 16.
(108) Alphonsus, C. S.; Rodseth, R. N. The Endothelial Glycocalyx: A Review of the Vascular Barrier. *Anaesthesia* **2014**, *69*, 777−784.
(109) Windhues, T.; Borchard, W. Effect of Acetylation on Physico-Chemical Properties of Bacterial and Algal Alginates in Physiological Sodium Chloride Solutions Investigated with Light Scattering Techniques. *Carbohydr. Polym.* **2003**, *52*, 47−52.
(110) Abraham, M. J.; Murtola, T.; Schulz, R.; Páll, S.; Smith, J. C.; Hess, B.; Lindahl, E. Gromacs: High Performance Molecular Simulations through Multi-Level Parallelism from Laptops to Supercomputers. *SoftwareX* **2015**, *1*−*2*, 19−25.
(111) Hockney, R.; Eastwood, J. *Computer Simulations Using Particles*; CRC Press, 1981.
(112) Hess, B.; Bekker, H.; Berendsen, H. J. C.; Fraaije, J. G. E. M. LINCS: A Linear Constraint Solver for Molecular Simulations. *J. Comput. Chem.* **1997**, *18*, 1463−1472.
(113) Berendsen, H. J. C.; Grigera, J. R.; Straatsma, T. P. The Missing Term in Effective Pair Potentials. *J. Phys. Chem.* **1987**, *91*, 6269−6271.
(114) Plazinski, W.; Lonardi, A.; Hünenberger, P. H. Revision of the GROMOS 56A6CARBOforce field: Improving the description of ring-conformational equilibria in hexopyranose-based carbohydrates chains. *J. Comput. Chem.* **2016**, *37*, 354−365.
(115) Project, E.; Nachliel, E.; Gutman, M. Parameterization of Ca2+−Protein Interactions for Molecular Dynamics Simulations. *J. Comput. Chem.* **2008**, *29*, 1163−1169.
(116) Oostenbrink, C.; Villa, A.; Mark, A. E.; Van Gunsteren, W. F. A Biomolecular Force Field Based on the Free Enthalpy of Hydration and Solvation: The GROMOS Force-Field Parameter Sets 53A5 and 53A6. *J. Comput. Chem.* **2004**, *25*, 1656−1676.
(117) Mark, P.; Nilsson, L. Structure and Dynamics of the TIP3P, SPC, and SPC/E Water Models at 298 K. *J. Phys. Chem. A* **2001**, *105*, 9954−9960.
(118) Lima, M. P. M.; Nader, M.; Santos, D. E. S.; Soares, T. A. Compatibility of GROMOS-Derived Atomic Parameters for Lipopolysaccharide Membranes with the SPC/E Water Model and Alternative Long-Range Electrostatic Treatments Using Single Nonbonded Cutoff and Atom-Based Charge Schemes. *J. Braz. Chem. Soc.* **2019**, *30*, 2219−2230.
(119) Tsimpanogiannis, I. N.; Jamali, S. H.; Economou, I. G.; Vlugt, T. J. H.; Moultos, O. A. On the validity of the Stokes-Einstein relation for various water force fields. *Mol. Phys.* **2020**, *118*, No. e1702729.
(120) Riniker, S. Fixed-Charge Atomistic Force Fields for Molecular Dynamics Simulations in the Condensed Phase: An Overview. *J. Chem. Inf. Model.* **2018**, *58*, 565−578.
(121) Gebhardt, J.; Kleist, C.; Jakobtorweihen, S.; Hansen, N. Validation and Comparison of Force Fields for Native Cyclodextrins in Aqueous Solution. *J. Phys. Chem. B* **2018**, *122*, 1608−1626.
(122) Plazinski, W.; Lonardi, A.; Hünenberger, P. H. Revision of the GROMOS 56A6CARBOforce field: Improving the description of ring-conformational equilibria in hexopyranose-based carbohydrates chains. *J. Comput. Chem.* **2016**, *37*, 354−365.
(123) Maciel, B.; Oelschlaeger, C.; Willenbacher, N. Chain Flexibility and Dynamics of Alginate Solutions in Different Solvents. *Colloid Polym. Sci.* **2020**, *298*, 791−801.
(124) Martínez, L.; Andrade, R.; Birgin, E. G.; Martínez, J. M. Packmol: A Package for Building Initial Configurations for Molecular Dynamics Simulations. *J. Comput. Chem.* **2009**, *30*, 2157−2164.
(125) Eisenhaber, F.; Lijnzaad, P.; Argos, P.; Sander, C.; Scharf, M. The Double Cubic Lattice Method: Efficient Approaches to Numerical Integration of Surface Area and Volume and to Dot Surface Contouring of Molecular Assemblies. *J. Comput. Chem.* **1995**, *16*, 273−284.
(126) Bondi, A. Van Der Waals Volumes and Radii. *J. Phys. Chem.* **1964**, *68*, 441−451.
(127) Sorichetti, V.; Hugouvieux, V.; Kob, W. Determining the Mesh Size of Polymer Solutions via the Pore Size Distribution. *Macromolecules* **2020**, *53*, 2568−2581.
(128) Underwood, T. R.; Bourg, I. C. Large-Scale Molecular Dynamics Simulation of the Dehydration of a Suspension of Smectite Clay Nanoparticles. *J. Phys. Chem. C* **2020**, *124*, 3702−3714.
(129) Linse, J. B.; Hub, J. S. Three- And Four-Site Models for Heavy Water: SPC/E-HW, TIP3P-HW, and TIP4P/2005-HW. *J. Chem. Phys.* **2021**, *154*, 194501.
(130) Widom, B. Potential-Distribution Theory and the Statistical Mechanics of Fluids. *J. Phys. Chem.* **1982**, *86*, 869−872.
(131) Shah, J. K.; Asthagiri, D.; Pratt, L. R.; Paulaitis, M. E. Balancing Local Order and Long-Ranged Interactions in the Molecular Theory of Liquid Water. *J. Chem. Phys.* **2007**, *127*, 144508.
(132) Widom, B. Some Topics in the Theory of Fluids. *J. Chem. Phys.* **1963**, *39*, 2808−2812.

https://doi.org/10.1021/acs.jpcb.2c07129
J. Phys. Chem. B 2023, 127, 1828−1841

(133) Schneck, E.; Sedlmeier, F.; Netz, R. R. Hydration Repulsion between Biomembranes Results from an Interplay of Dehydration and Depolarization. *Proc. Natl. Acad. Sci. U.S.A.* **2012**, *109*, 14405−14409.
(134) Jaiswal, J. K. Calcium − How and Why? *J. Biosci.* **2001**, *26*, 357−363.
(135) Nishikawa, M.; Kobayashi, K. Calcium Prevents Biofilm Dispersion in Bacillus Subtilis. *J. Bacteriol.* **2021**, *203*, No. e0011421.
(136) Wang, T.; Flint, S.; Palmer, J. Magnesium and Calcium Ions: Roles in Bacterial Cell Attachment and Biofilm Structure Maturation. *Biofouling* **2019**, *35*, 959−974.
(137) Tsai, C. C.; Morrow, B. H.; Chen, W.; Payne, G. F.; Shen, J. Toward Understanding the Environmental Control of Hydrogel Film Properties: How Salt Modulates the Flexibility of Chitosan Chains. *Macromolecules* **2017**, *50*, 5946−5952.
(138) *CRC Handbook of Chemistry and Physics: A Ready-Reference Book of Chemical and Physical Data*, 85th ed.; Lide, D. R., Ed.; CRC Press: Boca Raton, FL, 2005.
(139) Hermans, J.; Pathiaseril, A.; Anderson, A. Excess Free Energy of Liquids from Molecular Dynamics Simulations. Application to Water Models. *J. Am. Chem. Soc.* **1988**, *110*, 5982−5986.
(140) Dömötör, G.; Hentschke, R. Atomistically Modeling the Chemical Potential of Small Molecules in Dense Systems. *J. Phys. Chem. B* **2004**, *108*, 2413−2417.
(141) Anwar, J.; Heyes, D. M. Robust and Accurate Method for Free-Energy Calculation of Charged Molecular Systems. *J. Chem. Phys.* **2005**, *122*, 224117.
(142) Kristóf, T.; Rutkai, G. Chemical Potential Calculations by Thermodynamic Integration with Separation Shifting in Adaptive Sampling Monte Carlo Simulations. *Chem. Phys. Lett.* **2007**, *445*, 74−78.
(143) Albaridi, N. A. Antibacterial Potency of Honey. *Int. J. Microbiol.* **2019**, *2019*, 2464507.
(144) Langmuir, I. Repulsive Forces Between Charged Surfaces in Water, and the Cause of the Jones-Ray Effect. *Science* **1938**, *88*, 430−432.
(145) Derjaguin, B.; Landau, L. Theory of the Stability of Strongly Charged Lyophobic Sols and of the Adhesion of Strongly Charged Particles in Solutions of Electrolytes. *Prog. Surf. Sci.* **1993**, *43*, 30−59.
(146) Pashley, R. M. Multilayer Adsorption of Water on Silica: An Analysis of Experimental Results. *J. Colloid Interface Sci.* **1980**, *78*, 246−248.
(147) Sun, E. W. H.; Bourg, I. C. Molecular Dynamics Simulations of Mineral Surface Wettability by Water versus CO2: Thin Films, Contact Angles, and Capillary Pressure in a Silica Nanopore. *J. Phys. Chem. C* **2020**, *124*, 25382−25395.
(148) Sauter, J.; Grafmüller, A. Predicting the Chemical Potential and Osmotic Pressure of Polysaccharide Solutions by Molecular Simulations. *J. Chem. Theory Comput.* **2016**, *12*, 4375−4384.
(149) Ido, N.; Lybman, A.; Hayet, S.; Azulay, D. N.; Ghrayeb, M.; Liddawieh, S.; Chai, L. Bacillus Subtilis Biofilms Characterized as Hydrogels. Insights on Water Uptake and Water Binding in Biofilms. *Soft Matter* **2020**, *16*, 6180−6190.
(150) Nielsen, L.; Li, X.; Halverson, L. J. Cell-Cell and Cell-Surface Interactions Mediated by Cellulose and a Novel Exopolysaccharide Contribute to Pseudomonas Putida Biofilm Formation and Fitness under Water-Limiting Conditions. *Environ. Microbiol.* **2011**, *13*, 1342−1356.
(151) Gulez, G.; Altıntaş, A.; Fazli, M.; Dechesne, A.; Workman, C. T.; Tolker-Nielsen, T.; Smets, B. F. Colony morphology and transcriptome profiling of Pseudomonas putida KT2440 and its mutants deficient in alginate or all EPS synthesis under controlled matric potentials. *MicrobiologyOpen* **2014**, *3*, 457−469.
(152) Roberson, E. B.; Firestone, M. K. Relationship between Desiccation and Exopolysaccharide Production in a Soil Pseudomonas Sp. *Appl. Environ. Microbiol.* **1992**, *58*, 1284−1291.
(153) Lebre, P. H.; De Maayer, P.; Cowan, D. A. Xerotolerant Bacteria: Surviving through a Dry Spell. *Nat. Rev. Microbiol.* **2017**, *15*, 285−296.
(154) Comert, F.; Malanowski, A. J.; Azarikia, F.; Dubin, P. L. Coacervation and Precipitation in Polysaccharide-Protein Systems. *Soft Matter* **2016**, *12*, 4154−4161.
(155) Sing, C. E.; Perry, S. L. Recent Progress in the Science of Complex Coacervation. *Soft Matter* **2020**, *16*, 2885−2914.

https://doi.org/10.1021/acs.jpcb.2c07129
J. Phys. Chem. B 2023, 127, 1828−1841